Volume 5 | Number 4 | April 2015 | Pages 1973–2504

Catalysis Science & Technology

www.rsc.org/catalysis

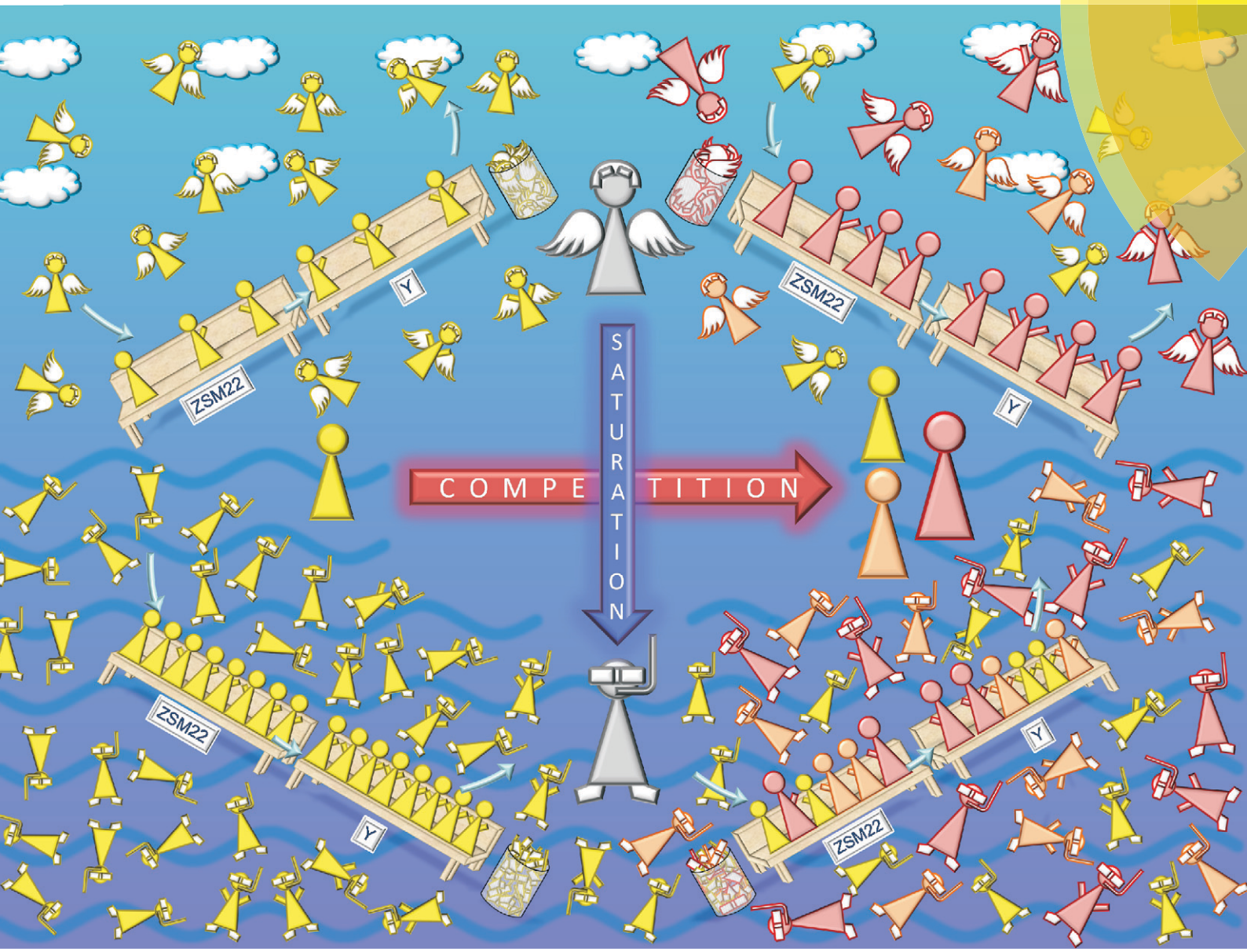

ISSN 2044-4753

ROYAL SOCIETY OF CHEMISTRY

COMMUNICATION

J. W. Thybaut *et al.*

Maximizing *n*-alkane hydroisomerization: the interplay of phase, feed complexity and zeolite catalyst mixing

Catalysis Science & Technology

COMMUNICATION

View Article Online
View Journal | View Issue

Cite this: *Catal. Sci. Technol.*, 2015, 5, 2053

Received 1st September 2014,
Accepted 23rd September 2014

DOI: 10.1039/c4cy01135j

www.rsc.org/catalysis

Maximizing *n*-alkane hydroisomerization: the interplay of phase, feed complexity and zeolite catalyst mixing†

B. D. Vandegehuchte,[a] J. W. Thybaut,*[a] J. A. Martens[b] and G. B. Marin[a]

Mixing of zeolites with different pore sizes enhances the yield of skeletal isomers from pure *n*-alkanes, but this synergic effect is limited in *n*-alkane mixtures because of preferential adsorption and cracking of the longest molecules. Single-Event MicroKinetic (SEMK) analysis reveals that enhanced yields of skeletal isomers can be obtained even with *n*-alkane mixtures, provided that the hydroisomerization reaction is performed under liquid-phase reaction conditions. Skeletal isomerization of linear alkanes is an essential process of fossil and renewable hydrocarbon fuel and lubricant production. The SEMK model enables the selection of optimum catalyst formulation and reaction conditions for superior paraffinic wax hydroconversion.

Current trends in fuel quality regulations prompt more advanced production processes for environmentally benign diesel and gasoline fuels exhibiting desired (ignition) properties. Medium-pore zeolites containing a one-dimensional pore structure, such as TON, MTT and AEL, have been established as ideal *n*-alkane hydroisomerization catalysts giving rise to 15–20% enhancement of the maximum isomer yield compared to non-shape selective catalysts.[1,2] The latter was rationalized in terms of the suppression of multibranched feed isomer formation at the pore mouths, while the active sites inside the pores remain exclusively accessible to linear alkanes.[3,4] Such shape-selective phenomena were denoted as 'pore mouth' and 'key lock' catalysis by Martens and co-workers,[5,6] who thoroughly investigated the product distributions obtained from heavy alkane hydroconversion on Pt/H–ZSM22. Although contested by a few other authors,[7,8] the establishment of pore mouth and key lock catalysis during *n*-alkane hydroconversion on unidirectional 10-membered pore zeolites was supported by separate physisorption measurements.[9,10] The elimination of micropore acid sites, accessible only to linear alkanes, was found crucial in optimizing the isomer selectivity of the catalyst, as elaborated from various synthesis studies.[11,12]

A further increase in maximum isomer yield could be achieved by physically mixing a ZSM22 (Si/Al = 45) zeolite with a non-shape selective Y (Si/Al = 2.6) zeolite, both loaded with 0.5 wt% Pt.[13] The observed synergy was explained through primary monobranching on the more active ZSM22, followed by secondary dibranched isomer formation on the more mildly active Y. The corresponding energy profiles are schematically represented in Fig. 1. Herein, the only relevant cracking mode on ZSM22, which is (s;p) β-scission of *n*-alkanes towards an unstable primary ion inside the micropores, is not shown. The pathway with the least resistance, *i.e.*, the lowest activation energies, is followed. As evident from the profile corresponding to the catalyst mixture depicted on the right, multibranching occurs exclusively on the Y zeolite after primary monobranching on ZSM22. This

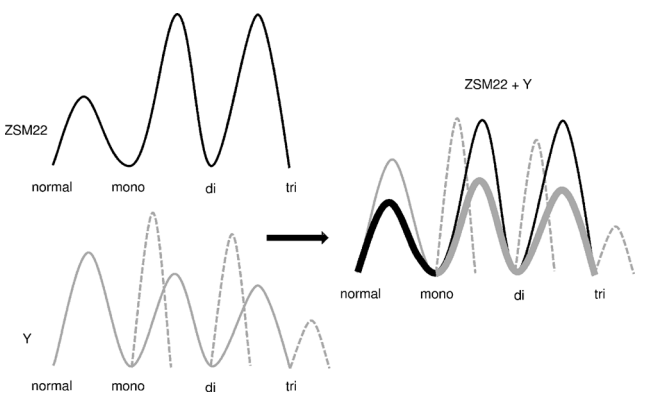

Fig. 1 Relative energy barriers in the isomerization (full lines) and cracking (dashed lines) of normal, mono-, di- and tribranched alkanes in their hydroconversion on Pt/H–ZSM22 (black), Pt/NaH–Y (gray), and a physical mixture of Pt/H–ZSM22 and Pt/NaH–Y (bold line, right).

[a] *Laboratory for Chemical Technology, Ghent University, Technologiepark 914, B-9052 Ghent, Belgium. E-mail: Joris.Thybaut@UGent.be; Tel: +32 9 331 17 52*
[b] *Centre for Surface Chemistry and Catalysis, KU Leuven, Kasteelpark Arenberg 23, B-3001 Heverlee, Belgium*

† Electronic supplementary information (ESI) available. See DOI: 10.1039/c4cy01135j

reaction sequence is also schematically depicted in Fig. 2-a. The activity of the Y zeolite should be tuned such that further isomerization toward tribranched species, which are susceptible to fast cracking,[14] is avoided.

By virtue of a fundamental Single-Event MicroKinetic (SEMK) model, Choudhury *et al.*[15] adequately simulated this synergy effect during *n*-decane hydroconversion by proportionally adding the net production rates, as evaluated on the individual catalysts, in accordance with the catalyst bed composition. The SEMK methodology, which is ideally suited to cope with complex reaction networks, relies on the concept of reaction families to reduce the number of model parameters while retaining its fundamental character. Physical phenomena, such as van der Waals forces between the reacting species and the catalyst framework, and bulk phase non-ideality are explicitly accounted for on top of the actual, intrinsic kinetics. This fundamental character of the model guarantees adequate extension from gas phase pure-component alkane data towards more industrially relevant conditions such as (complex) mixtures under liquid-phase conditions.[16–18]

The present work demonstrates how physisorption and phase effects can significantly conceal intrinsic reaction kinetics in hydroconversion. The synergy between a shape-selective and a non-shape selective zeolite is further explored for an *n*-alkane mixture under liquid-phase conditions *via* SEMK model simulations. The most important model assumptions imply:

1. Alkane physisorption occurs in the catalyst's micropores prior to any chemical reaction. Due to the narrow pore structure, any alkane entering the micropores experiences van der Waals interactions with mainly the pore walls, resulting in strong confinement; a multicomponent Langmuir isotherm could adequately describe this physisorption step.[19] The corresponding standard physisorption enthalpy and entropy losses are proportional to the component's carbon number. Because the latter is dominated by the former, the overall physisorption stabilization increases with increasing sorbate alkane number.[19]

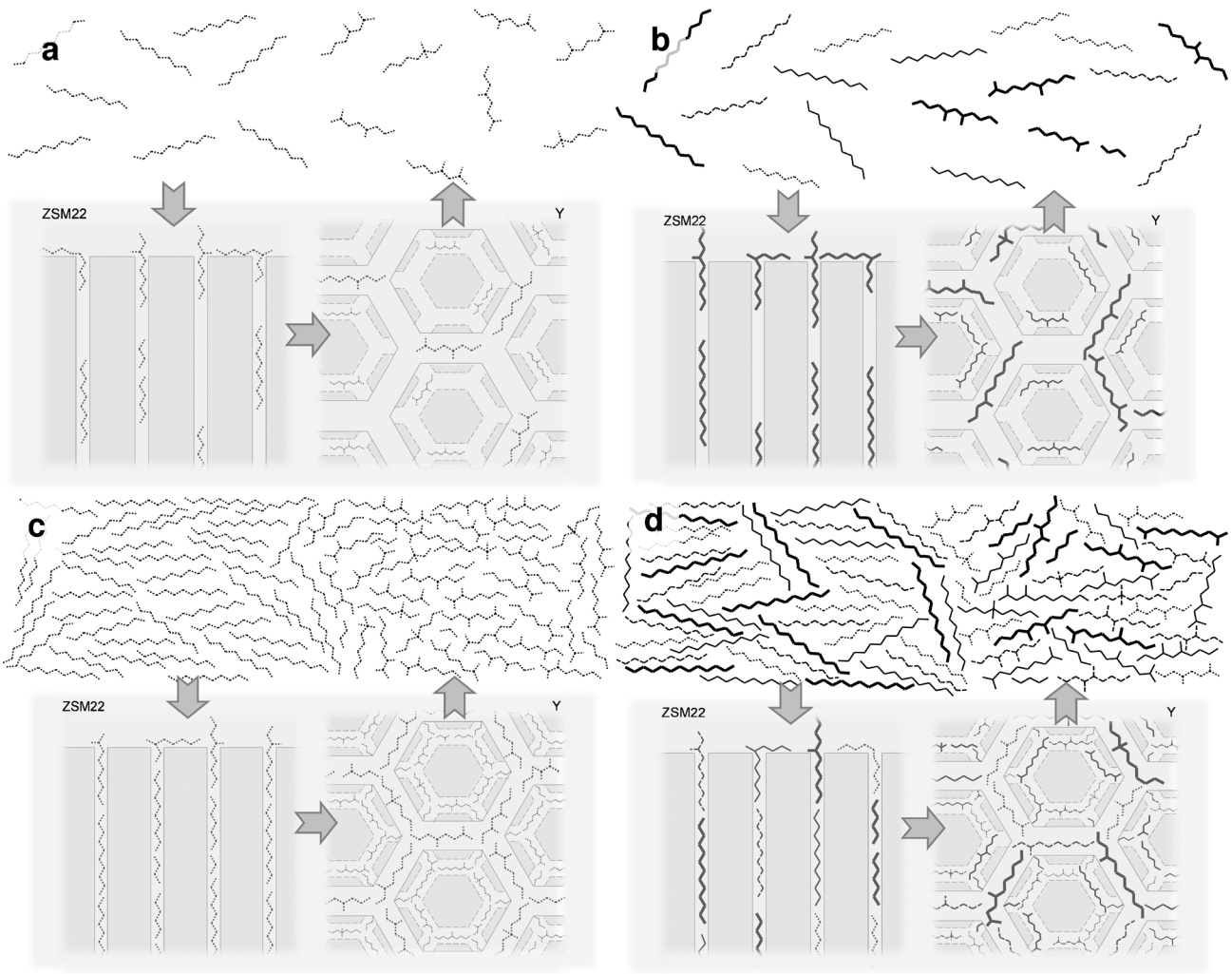

Fig. 2 Schematic representation of the effect of synergy between ZSM22 and Y on the total isomerization yield during *n*-decane (a and c) and parapur hydroconversion (b and d) under gas-phase (a and b) and liquid-phase conditions (c and d). Isomerization and cracking products of decane, undecane, dodecane and tridecane are represented as dotted, dashed, full and bold lines, respectively.

2. Dehydrogenation equilibrium is established between alkanes and alkenes by the metal sites, giving rise to the so-called 'ideal hydroconversion'.[20]

3. Alkene protonation at the catalyst's acid sites is quasi-equilibrated and can be described by means of a Langmuir isotherm-type expression.[20]

4. Isomerization *via* alkyl shift and PCP branching, and β-scission of carbenium ions act as the rate-determining steps in the catalytic cycles considered in the reaction network.[1]

5. The large number of elementary steps in the reaction network can be classified into a limited number of reaction families based on the type of reaction and the types of reactant and product carbenium ion involved. Unique, 'single-event' rate coefficients per reaction family reflect the actual chemistry involved in the reaction, while symmetry and chirality effects are separately accounted for by a factor called the 'number of single events'. More details on the SEMK methodology are available in recent work[21] and have been concisely summarized in the ESI.†

Bulk phase non-ideality, which is incorporated *via* a liquid-phase fugacity coefficient, primarily affects the physisorption step inside the zeolite pores.[16] Pore mouth and key lock mechanisms remain dominant in a reactive environment regardless of the phase of the feed,[22] even though branched alkanes might adopt a configuration at full saturation which allows them to enter the micropores of ZSM22.[23] The incorporation of phase and extreme shape selectivity phenomena in the present model is elaborated in more detail in the ESI.†

Initially, *n*-decane is considered as a feed, such as in earlier studies.[13,15] Next, the effects of the feed mixture and liquid bulk phase on the total isomer selectivity of physical Y–ZSM22 mixtures are systematically assessed by means of SEMK model simulations. To this purpose, the behavior of parapur, *i.e.*, a commercial mixture of *n*-alkanes with composition reported in Table 1,[17] was evaluated. Parapur is an adequate model feed for a Fischer–Tropsch wax primarily composed of *n*-alkanes which require a post-processing step to convert them into high-quality fuel blends.[24,25] By virtue of the SEMK methodology, the gap between gas- and liquid-phase conversion can be adequately bridged, which[17,18] consequently opens up the route towards SEMK-based screening of advanced catalytic materials under virtually any set of reaction conditions. The acquisition itself of intrinsic kinetic data under liquid bulk phase conditions and total feed conversions exceeding 90% remains a challenging task due to, *e.g.*, catalyst deactivation *via* coking.[26] Gas-to-liquid phase kinetic simulations have been proven however to provide an adequate representation of liquid-phase kinetic performance starting from gas phase data.[16,18]

Table 1 Molar composition of parapur. 'Trace' amounts of *n*-nonane and *n*-tetradecane are not included[17]

Component	Molar composition (%)
n-Decane (nC_{10})	17
n-Undecane (nC_{11})	43
n-Dodecane (nC_{12})	28
n-Tridecane (nC_{13})	12

SEMK simulation studies were carried out considering a 75–25, a 50–50 and a 25–75 wt% Y–ZSM22 mixture, in addition to the pure catalysts. ZSM22 and Y zeolites identical to those applied in the work of Choudhury *et al.*[15] were considered. The total isomerization yield is defined as the sum of all individual isomer yields:

$$Y_{iso} = \sum_{i=1}^{n_{iso}} Y_i = \sum_{i=1}^{n_{iso}} \frac{F_i}{F_{feed}^0} \quad (1)$$

Herein, Y_i represents the yield of isomer species i, as calculated from its outlet flow rate F_i relative to the inlet flow rate of the corresponding *n*-alkane feed. Outlet flow rates were calculated by adopting an ideal plug flow reactor model. Gas-phase experiments were simulated at 513 K and 1 MPa with an inlet H_2–nC_{10} molar ratio of 100. The space time was varied from 10 to 1250 kg s mol^{-1}, allowing simulation of the total isomerization yield in the entire range of feed conversion. While the effects of the reactor pressure and hydrogen inlet flow rate on the resulting product distribution are marginal, the reaction temperature significantly impacts the isomer selectivity of the ZSM22 catalyst. The latter stems from an increased contribution of (s;p) β-scission in the micropores at elevated temperatures. As will be shown later on, the reaction temperature serves as an important design parameter to maximize the total isomerization yield in *n*-alkane hydroconversion.

Fig. 3-a indicates the synergy that can be obtained for the total isomerization yield on Y–ZSM22 mixtures in the case of gas-phase *n*-decane hydroconversion.[13,15] The best performance is obtained with the catalyst mixture containing 75 wt% ZSM22. Simulation results using parapur as a feed indicate a maximum obtainable isomerization yield of only 34% and 60% on Y and ZSM22, respectively. A synergy effect between both catalysts, as observed during *n*-decane hydroconversion, remained practically absent, *vide* Fig. 3-b. This can be attributed to the molecular stabilization by physisorption being proportional to the carbon number of the species interacting with the catalyst framework,[26] see also Fig. 2-b. As a result, the conversion of nC_{13} occurs preferentially, followed by nC_{12} and nC_{11}, *vide* Fig. 4-a. Consequently, the total isomerization yield remains low compared to the individual isomer yields, certainly in case of Y, because heavier isomers are already cracked before lighter alkanes reach their maximum isomerization yield. This even induces a distinct inflection point in the corresponding total isomerization curve at a feed conversion of approximately 60%. Such a discrepancy is less pronounced on ZSM22 as the extent of cracking is considerably reduced by the shape selective behavior of the catalyst framework.

Liquid-phase effects were initially investigated using again *n*-decane as a feed. A total pressure of 9 MPa and an inlet H_2–nC_{10} ratio of 4 were applied while the reaction temperature again

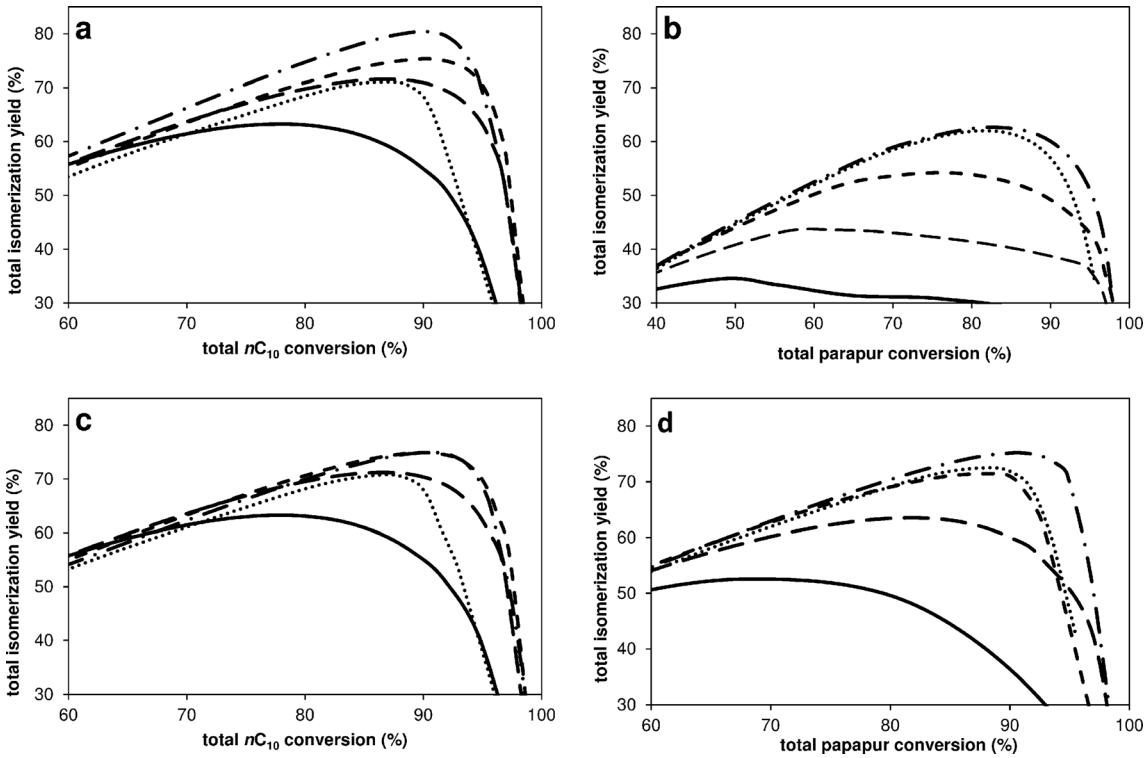

Fig. 3 Simulated total isomerization yield (eqn 1) at 513 K as a function of the total *n*-decane (a and c) or parapur conversion (b and d) from gas-phase (a and b) or liquid-phase hydroconversion (c and d) on Y (full), ZSM22 (dot), a 75–25 wt% (long dash), a 50–50 wt% (short dash) and a 25–75 wt% Y–ZSM22 mixture (dash dot), calculated using the SEMK model described in the ESI.†

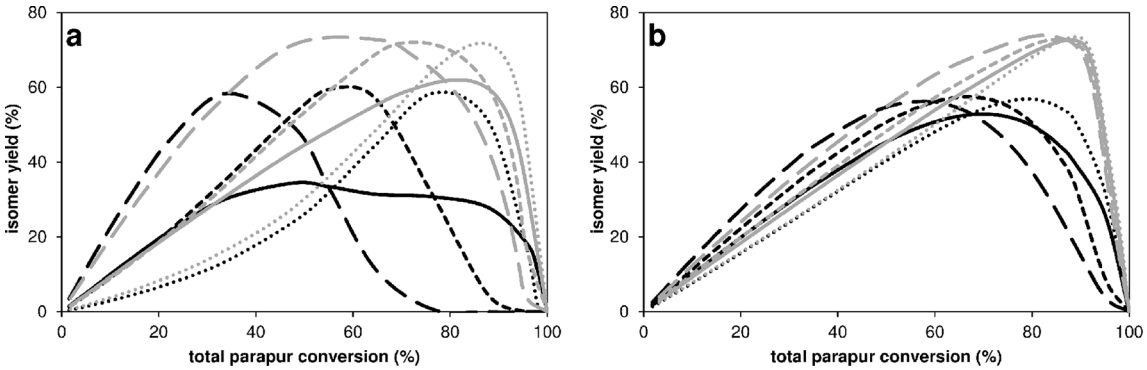

Fig. 4 Simulated total isomerization yield (full) and individual feed isomer yields (eqn 1) of C_{11} (dot), C_{12} (short dash) and C_{13} alkanes (long dash) as a function of the total feed conversion at 513 K on Y (black lines) and ZSM22 (gray lines) during the gas-phase reaction at 1 MPa (a) and the liquid-phase reaction at 6 MPa (b).

amounted up to 513 K. Compared to the results obtained under gas-phase conditions, Fig. 3-c shows a similar, yet more subtle increase in total isomerization yield when physical mixtures of both catalysts are used. Owing to the high hydrocarbon concentration under liquid-phase conditions, physisorption and reaction inside the catalyst micropores invariably occur in the saturation regime, *vide* Fig. 2-c. Saturation of the ZSM22 micropores in particular induces an increased contribution of (s;p) β-scission to the overall reaction kinetics, which in turn limits the global isomer yield and attenuates the synergy between both catalysts. Nevertheless, a synergy effect remains noticeable from the 50–50 wt% catalyst mixture onwards.

Apparently, mixture and liquid-phase effects are detrimental to the global isomerization affinity of Y–ZSM22 mixtures. Simulation of liquid-phase parapur hydroconversion considers both effects simultaneously; it was performed by adopting reaction conditions identical to those applied for an *n*-decane feed. Fig. 3-d shows a generally higher total isomerization yield compared to the results obtained from gas-phase parapur conversion for any of the catalysts and catalyst mixtures considered. The synergy between both catalysts surprisingly

re-emerges for the mixture containing 75 wt% ZSM22. As the intrinsic reaction kinetics is independent of the reactant bulk phase, other physical phenomena are responsible for the differences observed between gas- and liquid-phase hydroconversion of parapur. At micropore saturation under liquid-phase conditions, the extent of physisorption stabilization is not solely determined by the van der Waals forces between the sorbate and the sorbent (which favor the heavier hydrocarbons), but also by the intermolecular interactions between components with different carbon numbers.[16,27,28] The latter interactions primarily hamper the physisorption of the heaviest compounds, leading to a considerably increased contribution of the lighter species to the physisorbed phase.[26] In the case of a parapur feed, the preferred physisorption and subsequent reaction of C_{13} compounds, as observed during gas-phase reaction, have entirely vanished, see Fig. 2-d and 4-b, leading to maxima in individual alkane isomer yields, which nearly coincide with the maximum in total isomerization yield. Micropore saturation hence serves as a vital criterion to sustain the synergy between Y and ZSM22 when reverting to commercial paraffinic feeds.

The present simulation study nicely demonstrates how van der Waals forces govern the occurring intrinsic reaction kinetics as a function of the phase and feed composition. While the model gas-phase component experimentation is commonly preferred when evaluating the catalytic behavior, it remains crucial to quantitatively assess the mixture behavior under liquid-phase conditions. The present work convincingly illustrates how this can be achieved by modeling; moreover, conclusions purely based on gas-phase information may have resulted in the rejection of a potentially interesting physical catalyst mixture that can be used for converting *n*-alkane mixtures under liquid-phase conditions.

The versatility of the SEMK methodology is further demonstrated by the quantitative assessment of the total isomer yield which can be obtained as a function of the physical mixture composition and the temperature in liquid-phase parapur hydroconversion, see Fig. 5. The synergy between Y and ZSM22 is most obvious with catalyst mixtures mainly composed of the latter catalyst, *i.e.*, around 75 wt% at 460 K. As the reaction temperature increases, the optimal composition gradually moves toward 50–50 wt% at temperatures exceeding 540 K, owing to an enhanced contribution of cracking inside the ZSM22 micropores. The highest total isomerization yield is therefore obtained at the lowest temperature. Of course, an adequate trade-off needs to be made between this total isomer selectivity and the catalyst amount required to attain a sufficiently high feed conversion.

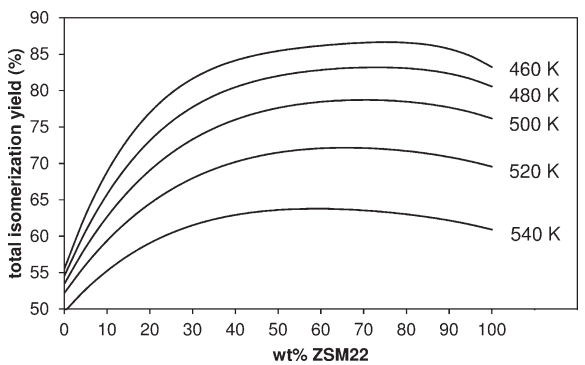

Fig. 5 Effect of reaction temperature and catalyst mixture composition on the maximum total isomerization yield (eqn 1) during liquid-phase parapur hydroconversion on Y–ZSM22 mixtures, simulated using the SEMK model elaborated in the ESI.†

Acknowledgements

This work was supported by the Research Board of Ghent University (BOF), the Interuniversity Attraction Poles Programme - Belgian State - Belgian Science Policy, by the European Research Council (ERC) under the European Union's Seventh Framework Programme (Grant FP7/2007-2013)/ERC Grant Agreement No. 615456, and the 'Long Term Structural Funding (Methusalem) by the Flemish Government' of GBM and JAM. FWO is acknowledged for project funding.

References

1 J. A. Martens, R. Parton, L. Uytterhoeven, P. A. Jacobs and G. F. Froment, *Appl. Catal.*, 1991, **76**, 95–116.
2 C. R. Marcilly, *Top. Catal.*, 2000, **13**, 357–366.
3 C. S. L. Narasimhan, J. W. Thybaut, G. B. Marin, J. A. Martens, J. F. Denayer and G. V. Baron, *J. Catal.*, 2003, **218**, 135–147.
4 C. S. L. Narasimhan, J. W. Thybaut, G. B. Marin, P. A. Jacobs, J. A. Martens, J. F. Denayer and G. V. Baron, *J. Catal.*, 2003, **220**, 399–413.
5 M. C. Claude and J. A. Martens, *J. Catal.*, 2000, **190**, 39–48.
6 M. C. Claude, G. Vanbutsele and J. A. Martens, *J. Catal.*, 2001, **203**, 213–231.
7 T. L. M. Maesen, M. Schenk, T. J. H. Vlugt, J. P. De Jonge and B. Smit, *J. Catal.*, 1999, **188**, 403–412.
8 T. L. M. Maesen, R. Krishna, J. M. Van Baten, B. Smit, S. Calero and J. M. C. Sanchez, *J. Catal.*, 2008, **256**, 95–107.
9 J. A. Martens, G. Vanbutsele, P. A. Jacobs, J. Denayer, R. Ocakoglu, G. Baron, J. A. M. Arroyo, J. Thybaut and G. B. Marin, *Catal. Today*, 2001, **65**, 111–116.
10 R. A. Ocakoglu, J. F. M. Denayer, G. B. Marin, J. A. Martens and G. V. Baron, *J. Phys. Chem. B*, 2003, **107**, 398–406.
11 K. Hayasaka, D. Liang, W. Huybrechts, B. R. De Waele, K. J. Houthoofd, P. Eloy, E. M. Gaigneaux, G. Van Tendeloo, J. W. Thybaut, G. B. Marin, J. F. M. Denayer, G. V. Baron, P. A. Jacobs, C. E. A. Kirschhock and J. A. Martens, *Chem. – Eur. J.*, 2007, **13**, 10070–10077.
12 J. A. Martens, D. Verboekend, K. Thomas, G. Vanbutsele, J. Perez-Ramirez and J. P. Gilson, *Catal. Today*, 2013, **218**, 135–142.
13 R. Parton, L. Uytterhoeven, J. A. Martens, P. A. Jacobs and G. F. Froment, *Appl. Catal.*, 1991, **76**, 131–142.
14 J. Weitkamp, *ChemCatChem*, 2012, **4**, 292–306.
15 I. R. Choudhury, J. W. Thybaut, P. Balasubramanian, J. F. M. Denayer, J. A. Martens and G. B. Marin, *Chem. Eng. Sci.*, 2010, **65**, 174–178.

16 C. S. L. Narasimhan, J. W. Thybaut, J. A. Martens, P. A. Jacobs, J. F. Denayer and G. B. Marin, *J. Phys. Chem. B*, 2006, **110**, 6750–6758.
17 J. W. Thybaut, C. S. L. Narasimhan and G. B. Marin, *Catal. Today*, 2006, **111**, 94–102.
18 C. S. Raghuveer, J. W. Thybaut, R. De Bruycker, K. Metaxas, T. Bera and G. B. Marin, *Fuel*, 2014, **125**, 206–218.
19 J. F. M. Denayer and G. V. Baron, *Adsorption*, 1997, **3**, 251–265.
20 J. W. Thybaut, C. S. L. Narasimhan, J. F. Denayer, G. V. Baron, P. A. Jacobs, J. A. Martens and G. B. Marin, *Ind. Eng. Chem. Res.*, 2005, **44**, 5159–5169.
21 J. W. Thybaut and G. B. Marin, *J. Catal.*, 2013, **308**, 352–362.
22 C. S. L. Narasimhan, J. W. Thybaut, J. F. Denayer, G. V. Baron, P. A. Jacobs, J. A. Martens and G. B. Marin, *Ind. Eng. Chem. Res.*, 2007, **46**, 8710–8721.
23 J. F. Denayer, A. R. Ocakoglu, W. Huybrechts, J. A. Martens, J. W. Thybaut, G. B. Marin and G. V. Baron, *Chem. Commun.*, 2003, 1880–1881.
24 C. Bouchy, G. Hastoy, E. Guillon and J. A. Martens, *Oil Gas Sci. Technol.*, 2009, **64**, 91–112.
25 V. Calemma, C. Gambaro, W. O. Parker, R. Carbone, R. Giardino and P. Scorletti, *Catal. Today*, 2010, **149**, 40–46.
26 J. F. M. Denayer, B. De Jonckheere, M. Hloch, G. B. Marin, G. Vanbutsele, J. A. Martens and G. V. Baron, *J. Catal.*, 2002, **210**, 445–452.
27 G. L. Aranovich and M. D. Donohue, *Colloids Surf., A*, 2001, **187**, 95–108.
28 G. L. Aranovich and M. D. Donohue, *Langmuir*, 2003, **19**, 2722–2735.

